TENMAK BOREN

JOURNAL OF BORON
BOR DERGİSİ
https://dergipark.org.tr/boron



Thermoelectric properties of B_4C-SiC composites with various compositions and microstructures

Salih Çağrı Özer [1,*], **Mehmet Berke Yalaman** [1], **Servet Turan** [1,2]

[1] Eskişehir Technical University, Faculty of Engineering, Materials Science and Engineering Department, Eskişehir, 26555, Türkiye
[2] Ceramic Research Center, Eskişehir, 26555, Türkiye

ARTICLE INFO

Article History:
Received December 16, 2025
Accepted April 3, 2026
Available online September 30, 2026

Research Article

DOI: 10.30728/boron.1838513

Keywords:
Boron carbide
Composite
Silicon carbide
Spark plasma sintering
Thermoelectric

ABSTRACT

Nowadays, energy applications constitute the main causes of global problems such as environmental pollution, excessive energy consumption, and disproportionate use of non-renewable resources. Therefore, research and investments in the efficient use of energy, alternative renewable energy sources, and environmentally friendly practices are imperative. In energy efficiency applications, special attention must be paid to the thermoelectric properties of materials, including thermal stability, Seebeck coefficient, electrical conductivity, and thermal conductivity. In these applications, carbides such as B_4C and SiC are of great importance due to their tunable and effective thermoelectric properties at high temperatures. In this study, B_4C and SiC-based composites with various compositions were produced by using the spark plasma sintering method to examine and improve the temperature-dependent (573 K to 923 K) thermoelectric properties through the effect of the ratios of B_4C and SiC within the composition and powder or granule matrix.

1. Introduction

The high usage of non-renewable energy resources and industrial processes has led to increased environmental pollution, energy consumption, and costs, resulting in global warming and the energy crisis. The primary cause of these global-scale problems is energy-related practices. Therefore, the efficient use of energy, alternative renewable energy sources, and environmentally friendly applications have necessitated research and investment in these areas. Research today is focused on materials that offer improved performance/cost ratios and minimal environmental damage throughout their service life. In this regard, thermoelectric devices can directly convert heat into electricity and utilize thermal sources such as industrial waste heat and solar energy, without any moving parts or components. Consequently, the market share of thermoelectric technology in renewable energy continues to grow rapidly, along with the discovery of new market opportunities [1]. The efficiency of a thermoelectric material is measured by the thermoelectric figure of merit, ZT, which defines its maximum performance limitation, given below as Equation 1.

$$ZT=\frac{S^2\sigma}{\kappa}T \quad (1)$$

Where S represents the Seebeck coefficient (μV/K), σ represents the electrical conductivity (S/m), κ represents the thermal conductivity (W/mK), and T represents the absolute temperature (K). In thermoelectrics, special attention must be given to these properties, since a high Seebeck coefficient and electrical conductivity, or a highpower factor ($S^2\sigma$), in addition to a low thermal conductivity is required for a high ZT value [2]. There are two general approaches to enhance the thermoelectric efficiency of thermoelectric materials: (1) reducing the total thermal conductivity (κ_{tot}), given in Equation 2, and (2) enhancing the power factor [3].

$$\kappa_{tot}=\kappa_L+\kappa_e \quad (2)$$

Where κ_L and κ_e represent the lattice and the electronic contributions to the thermal conductivity, respectively [4].

Thermoelectric materials that function at high temperatures and are widely used can be classified into skutterudites, half-Heusler compounds, and Si-Ge alloys. Since these materials contain expensive and rare compounds, it is essential to explore alternative materials that do not include costly and rare constituents [5].

In this context, due to their remarkable properties, carbide and boride ceramic and ceramic-based composite materials, which are used in various

*Corresponding author: salihcagriozer@eskisehir.edu.tr

© 2026 Turkish Energy Nuclear and Mineral Research Agency
CC BY-NC-SA 4.0

applications such as energy storage, electronics, aviation, and space industries, might serve as effective substitutes as high-temperature thermoelectric materials. Their high electrochemical corrosion, thermal shock, and wear resistance, large Seebeck coefficients, good electrical and thermal transport properties, along with their thermal, chemical, and mechanical stability at high temperatures, make them environmentally friendly and cost-effective alternatives [6].

Among the carbide ceramics, B_4C [7], SiC [8], and TiC [9] have been the focus of research due to their tunable and effective thermoelectric properties at high temperatures [10]. Boron carbides, in particular, have drawn interest in thermoelectric applications due to their high Seebeck coefficient (≈250 μV/K) with high charge carrier densities (≈10^{21} cm^{-3}). Intermetallic borides with high boron content (>65%) exhibit great potential among well-known thermoelectric materials and can be used at extremely high temperatures, typically exceeding 1200 K, where commercially available thermoelectric materials are ineffective [10, 11].

However, the thermoelectric potential of B_4C is limited for several reasons: its low fracture toughness [12], and a low sinterability due to low surface diffusion rate and strong covalent bonding between boron and carbon. For nearly full densification, B_4C requires sintering at very high temperatures (>2200°C) [13]. Since the densification rate of monolithic B_4C is relatively low, making it is difficult to achieve more than 80% of its theoretical density through pressureless sintering [14]. To overcome these challenges, researchers have explored various secondary phases and additive materials (e.g., C, TiC, SiC, TiB_2, Si_3N_4) [15-18] combined with different sintering techniques, including pressureless sintering [12, 19], hot pressing [20, 21], hot isostatic pressing [22, 23], and spark plasma sintering (SPS) [24, 25]. SPS method simultaneously utilizes pressure and direct current during powder densification, under vacuum or an inert atmosphere. Thus, a higher heating rate, lower sintering temperature, and shorter sintering time could be achieved compared to the conventional sintering methods [26]. These properties and advantages make the SPS method an ideal process to consolidate hard-to-sinter carbide materials such as B_4C [27].

On the other hand, while B_4C exhibits high electrical and low thermal conductivities, SiC has a very high Seebeck coefficient, but needs enhanced electrical and thermal conductivities to be viable for thermoelectric applications. By combining SiC and B_4C powders in different ratios, these properties can be tailored as desired. Therefore, in theory, producing B_4C C-SiC composites addresses the low sinterability of B_4C. At the same time, it provides the electrical and thermal transport properties required for thermoelectric applications. As a result, these composites emerge as promising alternative materials for high-temperature thermoelectric applications [28, 29].

The aim of this study is to investigate the thermoelectric properties of B_4C-SiC composites with various compositions and optimize the production process by the spark plasma sintering method. Another objective is investigating the effect of raw material morphology on the thermoelectric properties of the composites. For this purpose, SiC in both granule and powder forms was mixed with B_4C powders in different ratios. Powder compositions were then spark plasma sintered at different sintering temperatures (1870-2120°C), dependent on composition, with a constant holding time of 10 minutes. The goal was to achieve B_4C-SiC composites with a high densification rate and improve thermoelectric performance.

2. Materials and Methods

2.1. Materials

B_4C powders (d_{50}=1.61 μm, >98%, CRS Chemicals, USA), SiC powders (d_{50}=0.45 μm, >99.99%, H. C. Starck, Germany) and as-received SiC granules (d_{50}=89.25 μm, 97.4%, Sika, Norway) were used as raw materials in this study.

2.2. Methods

B_4C-SiC powder mixtures were prepared by mechanical mixing with a planetary ball mill (Pulverisette 7, Fritsch, Germany) with a rotational speed of 300 rpm for 1 hour in a Si_3N_4 jar utilizingSi_3N_4 milling media, maintaining a mass ratio of 3:1 of ethanol to solid. Different compositions and sample denominations dependent on B_4C/SiC content are given in Table 1. Prepared suspensions were then placed in a rotary evaporator (Hei-VAP ML, Heidolph, Germany) to remove the liquid content. Dried powder mixtures were then sieved through a 75 μm sieve to eliminate any agglomerations.

Table 1. Sample denominations, compositions, and spark plasma sintering temperatures.

Sample Name	Composition (wt. %)			Sintering Temperature (°C)
	B_4C	SiC	SiC (granule)	
B_4C	100	-	-	1900
75B_4C25SiC	75	25	-	1970
70B_4C30SiC	70	30	-	1965
65B_4C35SiC	65	35	-	2000
65SiCG35B_4C	35	-	65	2125
65SiC35B_4C	35	65	-	2060
70SiC30B_4C	30	70	-	2060
75SiC25B_4C	25	75	-	2035
SiC	-	-	100	2090

Prepared powders were sintered in a spark plasma sintering furnace (HP 25D, FCT, Germany). Powders were wrapped in graphite foil to prevent direct contact between the powders and the graphite die.

Prior to sintering, 10 MPa pressure was applied for 30 seconds using a hand press. Spark plasma sintering process was carried out within a temperature range of 1900-2125°C under vacuum; the sintering temperature of each sample is given in Table 1. Sintering temperatures were determined during the sintering process by following the sintering curves for each composition to obtain the maximum densification. Although a general trend of increased sintering temperature with an increasing amount of SiC addition was observed, slight deviations from this trend were also observed. These deviations might be attributed to the temperature measurement systems used in SPS, where misalignment of the pyrometer and shifts of the die are two common problems of temperature measurement errors that affect the accuracy and the reproducibility of the experiments [30]. That's why the sintering temperature of each sample was determined by following the displacement/shrinkage curve to obtain maximum densification, instead of using predetermined sintering temperatures. Other sintering parameters, excluding the sintering temperature, remained the same for all the samples, with a heating rate of 100°C/min, uniaxial pressure of 40 MPa, and a holding time of 10 minutes.

Phase and microstructural analyses were carried out on the polished surfaces of the spark plasma sintered bulk samples. An X-ray diffractometer (XRD) was used to determine phase structure (Miniflex, Rigaku, Japan), measurements were conducted between 2Θ=20-80° with a scan speed of 2.0°/min. The microstructures were investigated by using backscatter electron imaging in scanning electron microscopy (SEM Supra 50VP, Zeiss, Germany).

Electrical conductivity and Seebeck coefficient measurements were conducted simultaneously by a thermoelectric analysis device, utilizing the four-point-probe method (LSR-3, Linseis, Germany). The measurements were performed in the 573-923 K temperature range under a He atmosphere, without applying any platinum or gold surface contact.

The thermal conductivity values of the sintered samples were calculated according to Equation 3, given below.

$$\kappa = \alpha c_p \rho \quad (3)$$

Where κ represents thermal conductivity (W/mK), α represents thermal diffusivity (mm^2/s), c_p represents heat capacity (J/gK), and ρ represents the bulk density (g/cm^3) of the sintered samples. Thermal diffusivity and heat capacity measurements were conducted by using the laser flash technique (LFA 457, Netzsch, Germany) under an Ar atmosphere in the 573-923 K temperature range. Bulk densities were measured by using Archimedes' method at room temperature. In addition to this, relative densities of the samples were calculated by the rule of mixtures to evaluate the densification during the spark plasma sintering process.

3. Results and Discussion

Sintering temperatures of each composition were determined during the spark plasma sintering process by following the sintering curves to obtain the maximum densification. Sintering temperatures of each composition are given in Table 1, as mentioned before. Bulk and relative densities of spark plasma sintered B_4C-SiC composites are shown in Figure 1. A general trend of an increase in both bulk and relative density values was observed with increasing SiC content. Small differences between the relative density values were observed depending on the composition. All the samples showed relative densities higher than 97%, with the lowest being the monolithic B_4C as 97.0% and the highest being $75B_4C25SiC$ as 98.9%. Relative densities of the composites decreased with higher amounts of B_4C content, where a relatively higher sintering temperature is needed for densification [31]. Samples with SiC content higher than 30% required sintering temperatures above 2000°C. When the densification of samples with the same composition but different morphologies was evaluated, it was observed that the sample $65SiCG35B_4C$ required a higher sintering temperature than $65SiC35B_4C$, and relative densities of 98.2% and 98.6% were obtained, respectively.

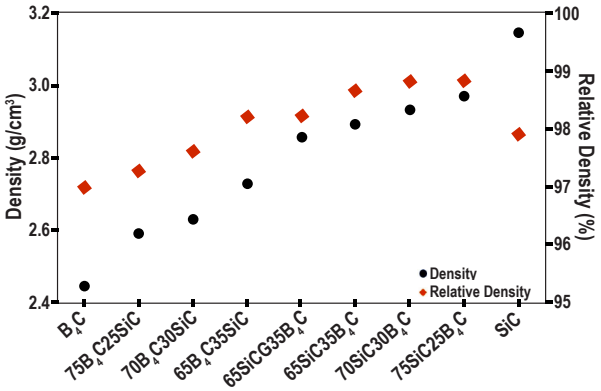


Figure 1. Bulk and relative density values of spark plasma sintered B_4C-SiC composites.

XRD patterns of sintered bulk samples of B_4C-SiC ceramic composites are given in Figure 2. XRD analysis revealed only peaks corresponding to SiC and B_4C, with no additional phases detected, meaning no interaction occurred between the raw materials of SiC and B_4C during sintering. In addition to this, XRD patterns showed that both the 6H and 4H polytypes of SiC are present in the samples. Intensities of 6H and 4H-SiC peaks increase with increasing SiC content, whereas intensities of B_4C peaks decrease, and vice versa.

Microstructures of B_4C-SiC composites are given in Figure 3, where Figure 3 (b, c) is the B_4C-rich sample and Figure 3 (d, e) is the SiC-rich sample. Light gray phases represent SiC, whereas black phases represent B_4C, as confirmed by the energy dispersive X-ray spectroscopy (EDS) analysis given

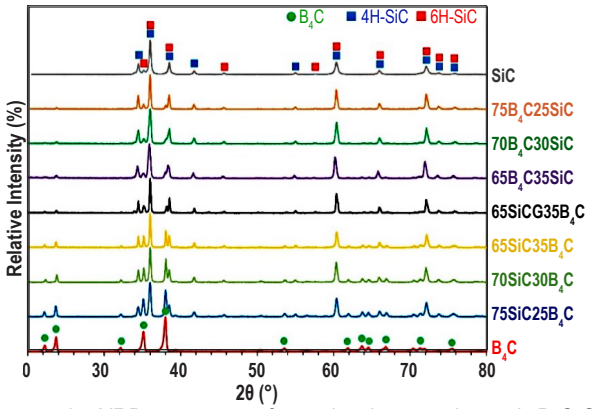


Figure 2. XRD patterns of spark plasma sintered B_4C-SiC composites.

in Figure 3 (a). Regardless of the composition, SiC and B_4C phases were homogeneously distributed within the microstructure, with small amounts of both B_4C and SiC agglomerations present. A small amount of porosity was observed within the microstructures, consistent with the relative density values given in Figure 1.

Figure 4 shows the microstructures of the 65SiC35B_4C powder and 65SiCG35B_4C granule matrix composites comparatively. When the microstructures of composites sintered with SiC powders (Figure 4 (a)) and SiC granules (Figure 4 (b)) were investigated, SiC granule clusters and B_4C phase densities at the granule boundaries were observed. Small amounts of porosities can also be found within the SiC granules, which may be caused by the difference in densification between the SiC matrix and B_4C boundary regions. This densification can be explained by the localization of the spark plasma sintering current density on the B_4C phase due to the high electrical conductivity difference between the SiC and B_4C phases [32].

Electrical transport properties dependent on composition and temperature were plotted in Figure 5. The electrical conductivity values of the sintered samples in the temperature range of 573-923 K, given in Figure 5 (a), showed that the electrical conductivity of all samples increased with increasing temperature, indicating typical semiconductor behavior [6]. It was observed that the electrical conductivity increases as the B_4C content in the composition increases. This is due to the much higher electrical conductivity of B_4C compared to SiC. A maximum electrical conductivity value of ≈4625 S/m was obtained with the sample 75B_4C25SiC at 923 K, a value approximately two orders of magnitude higher than pristine SiC and ≈30% lower than pristine B_4C. On the other hand, the lowest value obtained was ≈230 S/m with the sample 75SiC25B_4C, which is approximately three times higher than the monolithic SiC.

The electrical conductivity of the SiC powder-B_4C powder composite 65SiC35B_4C is ≈1530 S/m at 923 K, whereas the electrical conductivity of the SiC granule matrix composite 65SiCG35B_4C at the same temperature is ≈1190 S/m. When these two samples are compared, it can be inferred that changing the matrix from powder to granule leads to a significant decrease in electrical conductivity values, which may be explained by the bigger SiC phase regions indirectly reducing electrical conductivity by trapping charge carriers at SiC grains and reducing the number of free charge carriers or dropping their mobility by blocking the conductive B_4C pathways [33]. Another explanation for this may be the porosities present inside the SiC granules, which were observed by the SEM images given in Figure 4 (b), as well as the lower relative density values given in Figure 1. Since porosities act as electron scattering centers, a slightly more porous 65SiCG35B_4C sample would have lower electrical conductivity [34].

The Seebeck coefficient values of the sintered samples in the temperature range of 573-923 K are shown in Figure 5 (b). If the Seebeck coefficient increases proportionally with temperature, it exhibits p-type behavior, indicating that the charge carriers are electron holes. Conversely, if the Seebeck coefficient decreases inversely with temperature, it exhibits n-type behavior, meaning that the charge carriers are electrons. The Seebeck coefficients between 573 and 923 K were observed to be increasing with increasing temperature for all samples, indicating a p-type semiconductor behavior and the dominant charge carriers as electron holes. It was observed that the Seebeck coefficient values of all the composites are higher than those of monolithic B_4C and lower than SiC, throughout the temperature range. Regardless of whether the matrix is B_4C or SiC, the Seebeck coefficient values increase with the increasing SiC ratio. This may be attributed to the increased carrier scattering, causing a reduction in carrier mobility by increasing the amount of SiC in the system, increasing the Seebeck coefficient while reducing the electrical conductivity [33], which is in conjunction with the lower electrical conductivity values observed with the samples with higher SiC content, as seen in Figure 5 (a). A maximum Seebeck coefficient of ≈350 μV/K was obtained with the sample 75SiC25B_4C at 923 K, a value ≈55% higher than pristine B_4C and ≈35% lower than pristine SiC, whereas the lowest value obtained was ≈240 μV/K with the sample 75B_4C25SiC, which is ≈5% higher than the monolithic B_4C.

It was observed that the SiC granule matrix composite 65SiCG35B_4C showed ≈3% higher Seebeck coefficient than the SiC powder-B_4C powder composite 65SiC35B_4C. These values are in conjunction with the electrical conductivity results, since electrical conductivity and Seebeck coefficient have an adverse relationship due to Mott's relation [35]. The phenomena explained above, affecting the electrical conductivity of 65SiCG35B_4C adversely, had a positive effect on the Seebeck coefficient.

The power factor values of the sintered samples in the temperature range of 573-923 K are shown in Figure 5 (c). The highest and the lowest power factor

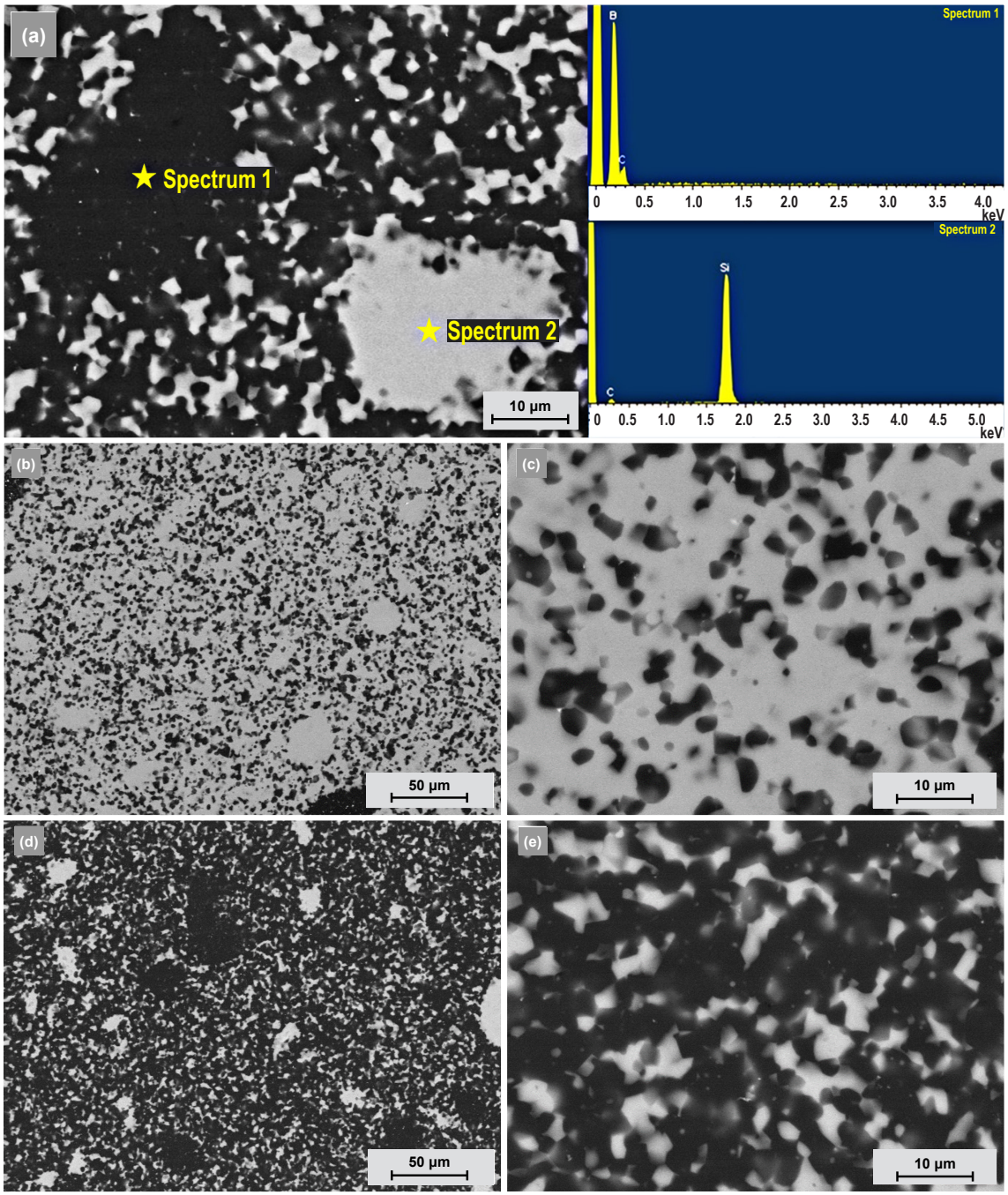


Figure 3. (a) SEM image and corresponding EDS patterns of different phases present in the sample with 35% SiC; SEM images of the sintered samples with compositions of (b, c) 25% B_4C and 75% SiC and (d, e) 70% B_4C and 30% SiC.

values at 923 K were obtained with the $75B_4C25SiC$ sample as $3.6x10^{-4}$ W/mK^2, and the $75SiC25B_4C$ sample as $2.8x10^{-5}$ W/mK^2, respectively. Despite the Seebeck coefficient having more effect on the power factor than the electrical conductivity, and SiC having higher Seebeck coefficient values compared to B_4C, the power factor values of the SiC-rich composites are lower, since these enhanced Seebeck coefficients did not compensate for the reduced electrical conductivities.

The power factor values of the SiC powder-B_4C powder composite $65SiC35B_4C$ and the SiC granule matrix composite $65SiCG35B_4C$ are $1.1x10^{-4}$ W/mK^2 and $1.3x10^{-4}$ W/mK^2, respectively, at 923 K. It is observed that the power factor of the $65SiC35B_4C$ is higher than the $65SiCG35B_4C$, since the enhanced electrical conductivity overcomes the lower Seebeck coefficient of the $65SiCG35B_4C$ sample.

Thermal transport properties dependent on composition and temperature were plotted in Figure 6. A monotonous decrease in both thermal diffusivity and conductivity was observed with increasing temperature for all of the samples. In addition to this, all composites showed thermal conductivity values between B_4C and SiC. Both thermal diffusivity and conductivity values are increasing with the increasing SiC content, due to

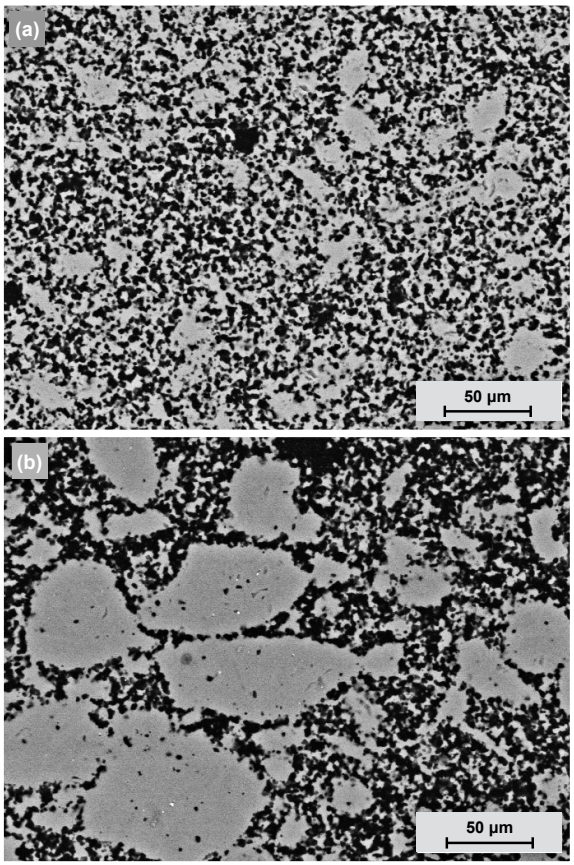


Figure 4. SEM images of the samples with different raw material morphologies: (a) sintered from powders and (b) sintered with B_4C powders and SiC granules.

the intrinsically high thermal conductivity of SiC [6]. A minimum thermal conductivity value of ≈3.6 W/mK was obtained with the sample $75B_4C25SiC$ at 923 K, a value ≈300% lower than pristine SiC and ≈10% higher than monolithic B_4C, whereas the highest value obtained was ≈10.8 W/mK with the sample $75SiC25B_4C$, which is ≈50% lower than the monolithic SiC. In general, introducing B_4C to the SiC matrix greatly increased the thermal performance of the composites, whereas the other way around had adversely affected the thermal conductivity of B_4C.

Interestingly, the SiC granule matrix composite $65SiCG35B_4C$ showed ≈7.5% lower thermal conductivity than the SiC powder-B_4C powder composite $65SiC35B_4C$; this may be caused by the lower densification rate of the $65SiCG35B_4C$ sample, forming porosities inside SiC granules, which promotes phonon scattering and lower thermal conductivity [34], which were observed in the SEM images given in Figure 4 (b).

In this work, B_4C-SiC composites with various compositions were produced to maximize the ZT value (Figure 7) of the materials for optimum thermoelectric performance. Despite the enhanced electrical and thermal transport properties of the composites, monolithic B_4C showed a ZT value of 3.05×10^{-2} at 923 K, higher than the B_4C-SiC composites, due to having both the highest electrical and lowest thermal

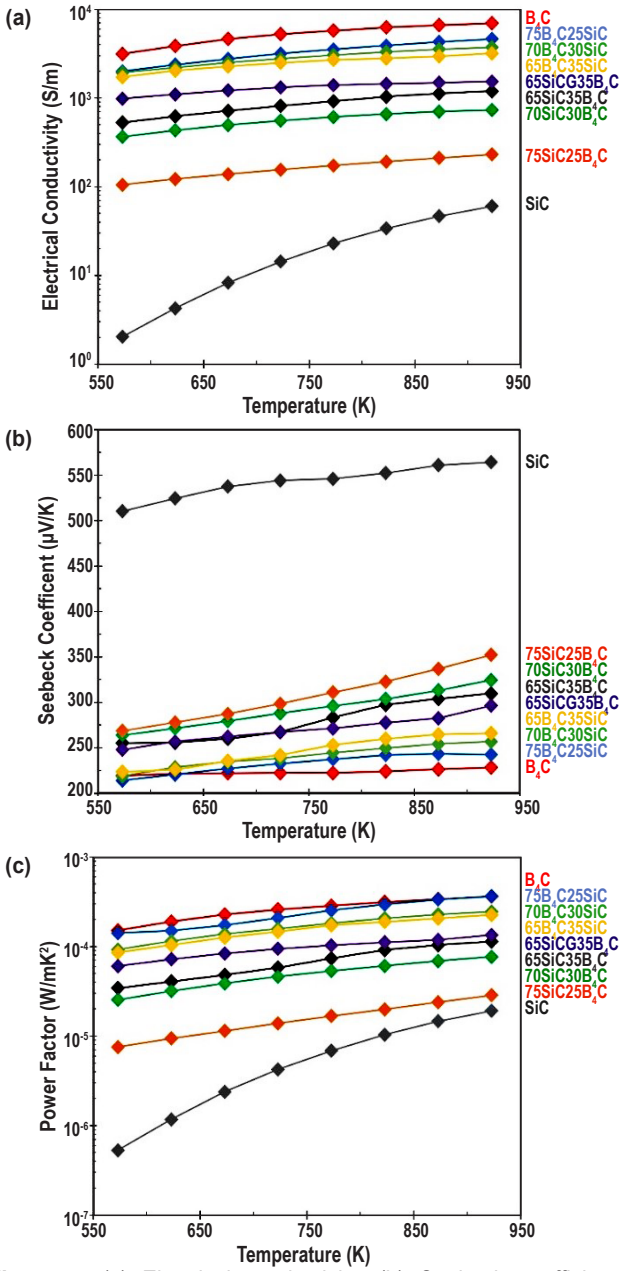


Figure 5. (a) Electrical conductivity, (b) Seebeck coefficient, and (c) power factor values of spark plasma sintered B_4C-SiC composites dependent on temperature.

conductivity values. On the contrary, monolithic SiC showed the lowest ZT values among all samples, with a maximum value of 2.91×10^{-4} at 923 K. The sample with the minimum addition of 25% B_4C improved the ZT value of SiC by approximately 110%, whereas the 75% B_4C addition improved the ZT value two orders of magnitude, to the ZT of 2.00×10^{-2} at 923 K. SiC-rich samples showed higher Seebeck coefficients, whereas B_4C-rich samples showed better electrical and thermal conductivity values. It was observed that forming a composite with B_4C improves the thermoelectric properties of SiC significantly.

Although there are other studies on the thermoelectric properties of B_4C-SiC composites, they did not mention any thermal conductivity or ZT values. These

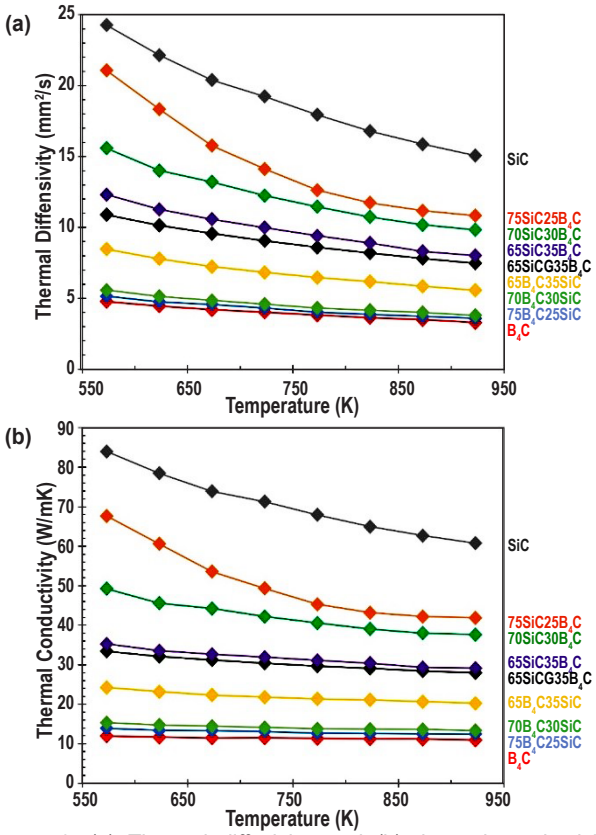


Figure 6. (a) Thermal diffusivity, and (b) thermal conductivity of spark plasma sintered B_4C-SiC composites dependent on temperature.

studies on the thermoelectric properties of B_4C-SiC composites are summarized in Table 2.

The study of Uehara et al. reported a high Seebeck coefficient value of ≈700 µV/K at 900°C by hot pressing B_4C and SiC powders [28]. The so-called synergistic enhancement of the Seebeck coefficient attributed to the fine defect structures was not observed in this study or other studies in the literature [29, 35, 36]. Ohba et al. pressureless sintered SiC with the addition of B_4C, C, and Al_2O_3 and obtained a high Seebeck coefficient of ≈500 µV/K and low electrical conductivity of 5.5×10^{-3} S/m [36]. Lankau et al. investigated the thermoelectric properties of pressureless sintered B_4C-SiC composites with various compositions, somewhat similar to this study. This study reported the highest Seebeck coefficient value of 390 µV/K

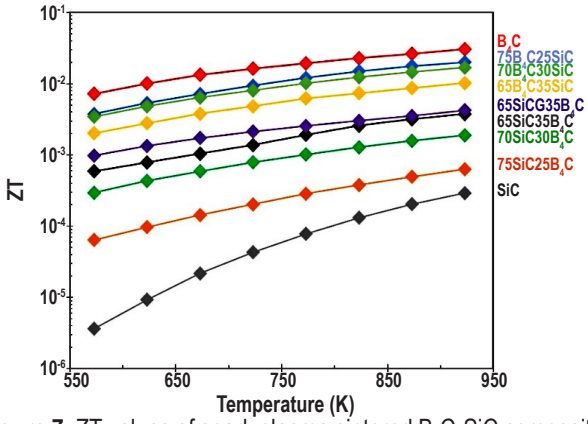


Figure 7. ZT values of spark plasma sintered B_4C-SiC composites dependent on temperature.

at 450°C with a composition of 40:60 B_4C to SiC ratio, albeit with a very low electrical conductivity of ≈5 S/m [29]. Feng et al. reported a ZT value of 0.036 at a higher temperature, 1000 K, with spark plasma sintered B_4C-Si-B composites. The resulting structure of B_xSiyC/SiC composites showed improved Seebeck coefficient and thermal conductivity values by increasing the carrier scattering due to the structural defects produced by the B_xSiyC ternary phase transformation [37]. Ozer et al. designed and fabricated a carrier scattering SiC network microstructure around B_4C granules rather than a classical particulate composite microstructure (as in this work and other studies from the literature). This designed SiC network had minimal adverse effects on electrical conductivity while simultaneously improving Seebeck coefficient and thermal conductivity, resulting in a record high ZT value of 0.12 for B_4C-based thermoelectric materials [35].

4. Conclusions

To investigate and compare the thermoelectric properties for high temperature applications (>650°C) of SiC/B_4C composites, SiC powders/granules, and B_4C powders in varying compositions were mixed and then sintered with the SPS process. XRD analysis only revealed the peaks of SiC (6H and 4H polytypes) and B_4C phases, indicating no occurrence of any reaction between the starting particles during sintering. Microstructural investigations showed that, regardless of the composition, SiC and B_4C were distributed

Table 2. Thermoelectric properties of B_4C-SiC based composites.

Composition		Production Method	Electrical Conductivity (S/m)	Seebeck Coeff. (µV/K)	Thermal Conductivity (W/mK)	ZT	Reference
B_4C	SiC						
30	70	Hot Press	-	700 (900°C)	-	-	[28]
5	95	Pressureless	3800 (800°C)	500 (800°C)	-	-	[36]
40	60	Pressureless	140 (450°C)	390 (450°C)	81.2 (55°C)	-	[29]
B_xSi_yC/SiC	SPS	4500 (1000K)	275 (1000K)	15 (1000K)	0.036 (1000K)	[37]	[37]
98	2	SPS	7800 (923K)	274 (923K)	4.3 (923K)	0.12 (923K)	[35]
75	25	SPS	4625 (923K)	242 (923K)	3.59 (923K)	0.02 (923K)	This work

homogeneously throughout the samples with minor local agglomerations. All of the compositions showed relative density values above 97%, with a general trend of increased densification by increasing the SiC content.

Electrical conductivities of all the samples increased with increasing temperature, indicating typical semiconductor behavior, and a general trend of increase is observed as the B_4C content in the composition increases, with a maximum electrical conductivity value of ≈4625 S/m with the sample $75B_4C25SiC$ and a minimum value of ≈230 S/m with the sample $75SiC25B_4C$ at 923K.

Vice versa, a general trend of decrease of the Seebeck coefficient was observed as the B_4C content increased, with maximum and minimum Seebeck coefficient values of ≈350 and ≈240 μV/K, with the samples $75SiC25B_4C$ and $75B_4C25SiC$, respectively, at 923K.

All composites showed thermal conductivity values between B_4C and SiC, and the thermal conductivity values are observed to be increasing with the increasing SiC content. A minimum thermal conductivity value of ≈3,6 W/mK was obtained with the sample $75B_4C25SiC$, whereas the highest value obtained was ≈10.8 W/mK with the sample $75SiC25B_4C$, at 923 K.

Overall, the ZT value of SiC was increased by the addition of B_4C, with the best value achieved with the sample $75B_4C25SiC$ as $2{,}00\times10^{-2}$ at 923 K, indicating that forming a composite with B_4C improves the thermoelectric properties of SiC significantly.

Although having lower ZT values than common high-temperature thermoelectric materials (such as skutterudites and half-Heusler alloys) for waste heat recovery from power plants, industrial processes, and the automobile industry, B_4C-SiC composites have high potential due to their high operational temperatures and can withstand large thermal differences between the hot and cold sides in a thermoelectric module [38].

5. Acknowledgements

This study was financially supported by the Scientific and Technological Research Council of Türkiye (TUBITAK) (219M514) and The Eskisehir Technical University Scientific Research Projects (20GAP058).

6. Author Contribution Statement

Salih Çağrı Özer: Methodology, data curation, data analysis, validation, writing review and editing.

Mehmet Berke Yalaman: Data curation, data analysis, writing original draft.

Servet Turan: Conceptualization, funding acquisition, methodology, project administration, supervision.

7. Conflict of Interest

The authors have no conflict of interest.

References

[1] Gayner, C., & Kar, K. K. (2016). Recent advances in thermoelectric materials. *Progress in Materials Science*, *83*, 330-382. https://doi.org/10.1016/j.pmatsci.2016.07.002

[2] Liu, W., Kim, H. S., Jie, Q., & Ren, Z. (2016). Importance of high-power factor in thermoelectric materials for power generation application: A perspective. *Scripta Materialia, 111*, 3-9. https://doi.org/10.1016/j.scriptamat.2015.07.045

[3] Zeier, W. G. (2017). New tricks for optimizing thermoelectric materials. Current Opinion in Green and Sustainable *Chemistry, 4*, 23-28. https://doi.org/10.1016/j.cogsc.2017.02.003

[4] Jia, N., Cao, J., Tan, X. Y., Dong, J., Liu, H., Tan, C. K. I., … & Suwardi, A. (2021). Thermoelectric materials and transport physics. *Materials Today Physics, 21*, 100519. https://doi.org/10.1016/j.mtphys.2021.100519

[5] Fitriani, Ovik, R., Long, B. D., Barma, M. C., Riaz, M., Sabri M. F. M., ... & Saidur, R. (2016). A review on nanostructures of high-temperature thermoelectric materials for waste heat recovery. *Renewable and Sustainable Energy Reviews, 64*, 635-659. https://doi.org/10.1016/j.rser.2016.06.035

[6] Ozer, S. C., Arslan, K., & Turan, S. (2024). Thermoelectric properties of carbide ceramics: A comparative analysis of thermoelectric properties of B4C, SiC and TiC. *Journal of the Australian Ceramic Society, 60*, 407-418. https://doi.org/10.1007/s41779-023-00979-4

[7] Bouchacourt, M., & Thevenot, F. (1985). The correlation between the thermoelectric properties and stoichiometry in the boron carbide phase B4C-B10.5C. *Journal of Materials Science, 20*, 1237-1247. https://doi.org/10.1007/BF01026319

[8] Kim, K. J., Jang, S. H., Kim, Y. W., Jang, B. K., & Nishimura, T. (2016). Conductive SiC ceramics fabricated by spark plasma sintering. *Ceramics International, 42*(15), 17892-17896. https://doi.org/10.1016/j.ceramint.2016.07.126

[9] Zhao, L., Qiu, W., Sun, Y., Chen, L., Deng, H., Yang, L., ... & Tang, J. (2021). Enhanced thermoelectric performance of Bi0.3Sb1.7Te3 based alloys by dispersing TiC ceramic nanoparticles. *Journal of Alloys and Compounds, 863*, 158376. https://doi.org/10.1016/j.jallcom.2020.158376

[10] Saglik, K., Mete, B., Terzi, I., Candolfi C., & Aydemir U. (2023). Thermoelectric borides: Review and future perspectives. *Advanced Physics Research, 2*(8), 2300010. https://doi.org/10.1002/apxr.202300010

[11] Sasaki, S., Takeda, M., Yokoyama, K., Miura, T., Suzuki, T., Suematsu, H., ... & Yatsui, K. (2005). Thermoelectric properties of boron-carbide thin film and thin film based thermoelectric device fabricated by intense-pulsed ion beam evaporation. *Science and Technology of Advanced Materials, 6*(2), 181-184. https://doi.org/10.1016/j.stam.2004.11.010

[12] Lee, H., & Speyer, R. F. (2004). Hardness and fracture toughness of pressureless sintered boron carbide

(B4C). *Journal of the American Ceramic Society, 85*(5), 1291-1293. https://doi.org/10.1111/j.1151-2916.2002.tb00260.x

[13] Martin, H. P., Feng B., & Michaelis, A. (2019). Pressureless sintering and properties of boron carbide composite materials. *International Journal of Applied Ceramic Technology, 17*(2), 407-412. https://doi.org/10.1111/ijac.13423

[14] Mashhadi, M., Taheri-Nassaj, E., & Sglavo, V. M. (2010). Pressureless sintering of boron carbide. *Ceramics International, 36*(1), 151-159. https://doi.org/10.1016/j.ceramint.2009.07.034

[15] Xu, C., Cai, Y., Flodström, K., Li, Z., Esmaeilzadeh, S., & Zhang, G. J. (2012). Spark plasma sintering of B4C ceramics: The effects of milling medium and TiB2 addition. *International Journal of Refractory Metals and Hard Materials, 30*(1), 139-144. https://doi.org/10.1016/j.ijrmhm.2011.07.016

[16] Levin, L., Frage, N., & Dariel, M. P. (1999). The effect of Ti and TiO2 additions on the pressureless sintering of B4C. *Metallurgical and Materials Transactions A, 30*, 3201–3210. https://doi.org/10.1007/s11661-999-0230-6

[17] Ayas, E., Kalemtas, A., Arslan, G., Kara, A., & Kara, F. (2008). Spark plasma sintering of Si3N4-B4C composites. *Journal of the Ceramic Society of Japan, 116*(1354), 727-731. https://doi.org/10.2109/jcersj2.116.727

[18] Sahin, F. C., Apak, B., Akin, I., Kanbur, H. E., Genckan, D. H., Turan, A., ... & Yücel, O. (2012). Spark plasma sintering of B4C–SiC composites. *Solid State Sciences, 14*(11-12), 1660-1663. https://doi.org/10.1016/j.solidstatesciences.2012.05.037

[19] Lee, H., & Speyer, R. F. (2004). Pressureless Sintering of boron carbide. *Journal of the American Ceramic Society, 86*(9), 1468-1473. https://doi.org/10.1111/j.1151-2916.2003.tb03498.x

[20] Chen, M. W., McCauley, J. W., LaSalvia, J. C., & Hemker, K. J. (2005). Microstructural characterization of commercial hot-pressed boron carbide ceramics. *Journal of the American Ceramic Society, 88*(7), 1935-1942. https://doi.org/10.1111/j.1551-2916.2005.00346.x

[21] Yue, X., Zhao, S., Lü, P., Chang, Q., & Ru, H. (2010). Synthesis and properties of hot pressed B4C–TiB2 ceramic composite. *Materials Science and Engineering: A, 527*(27-28), 7215-7219. https://doi.org/10.1016/j.msea.2010.07.101

[22] Cho, N., Bao, Z., & Speyer, R. F. (2005). Density- and hardness-optimized pressureless sintered and post-hot isostatic pressed B4C. *Journal of Materials Research, 20*, 2110-2116. https://doi.org/10.1557/JMR.2005.0260

[23] Yan, C., Xian, Y., Long, L., Luo, P., & Pang, X. (2023). Thermal properties of hot isostatic pressing Al/B4C composites with 50wt% B4C content. *Transactions of the Indian Institute of Metals, 76*, 2615-2623. https://doi.org/10.1007/s12666-023-02934-0

[24] Li, X., Jiang, D., Zhang, J., Lin, Q., Chen, Z., & Huang, Z. (2014). Densification behavior and related phenomena of spark plasma sintered boron carbide. *Ceramics International, 40*(3), 4359-4366. https://doi.org/10.1016/j.ceramint.2013.08.106

[25] Hayun, S., Kalabukhov, S., Ezersky, V., Dariel, M. P., & Frage, N. (2010). Microstructural characterization of spark plasma sintered boron carbide ceramics. *Ceramics International, 36*(2), 451-457. https://doi.org/10.1016/j.ceramint.2009.09.004

[26] Hu, Z. Y., Zhang, Z. H., Cheng, X. W., Wang, F. C., Zhang, Y. F., & Li, S. L. (2020). A review of multi-physical fields induced phenomena and effects in spark plasma sintering: Fundamentals and applications. *Materials & Design, 191*, 108662. https://doi.org/10.1016/j.matdes.2020.108662

[27] Biçer, H., Tuncer, M., Göçmez, H., Bogomol, I., Kolesnichenko, V., & Ragulya, A. (2024). Spark plasma sintering of boron carbide using Ti3SiC2 as a sintering additive. *Journal of Wuhan University of Technology-Materials Science Edition, 39*, 645-650. https://doi.org/10.1007/s11595-024-2921-7

[28] Uehara, M., Shiraishi, R., Nogami, A., Enomoto, N., & Hojo, J. (2004). SiC-B4C composites for synergistic enhancement of thermoelectric property. *Journal of the European Ceramic Society, 24*(2), 409-412. https://doi.org/10.1016/S0955-2219(03)00213-9

[29] Lankau, V., Martin, H. P, Hempel-Weber, R., Oeschler, N., & Michaelis, A. (2010). Preparation and thermoelectric characterization of SiC-B4C composites. *Journal of Electronic Materials, 39*, 1809-1813. https://doi.org/10.1007/s11664-010-1129-0

[30] Achenani, Y., Saadaoui, M., Cheddadi, A., & Fantozzi, G. (2017). Finite element analysis of the temperature uncertainty during spark plasma sintering: Influence of the experimental procedure. *Ceramics International, 43*(17), 15281-15287. https://doi.org/10.1016/j.ceramint.2017.08.067

[31] So, S. M., Choi, W. H., Kim, K. H., Park, J. S., Kim, M. S., Park, J., ... & Kim, H. S. (2020). Mechanical properties of B4C-SiC composites fabricated by hot-press sintering. *Ceramics International, 46*(7), 9575-9581. https://doi.org/10.1016/j.ceramint.2019.12.222

[32] Ozer, S. C. (2025). Enhanced thermoelectric properties of spark plasma sintered SiC with in-situ TiB2 network structures. *Ceramics International, 51*, 40022-40031. https://doi.org/10.1016/j.ceramint.2025.06.235

[33] Ozer, S. C., Arslan, K., Bircan, S., & Turan, S. (2024). Improved thermoelectric properties of spark plasma sintered B4C with SiC-segregated network structures. *Journal of Alloys and Compounds, 978*, 173520. https://doi.org/10.1016/j.jallcom.2024.173520

[34] Kultayeva, S., Ha, J. H., Malik, R., Kim, Y. W., & Kim, K. J. (2020). Effect of porosity on electrical and thermal conductivities of porous SiC ceramics, *Journal of the European Ceramic Society, 40*(4), 996-1004. https://doi.org/10.1016/j.jeurceramsoc.2019.11.045

[35] Ozer, S. C., Arslan, K., Bircan, S., & Turan, S. (2024). Improved thermoelectric properties of spark plasma sintered B4C with SiC-segregated network structures. *Journal of Alloys and Compounds, 978*, 173520. https://doi.org/10.1016/j.jallcom.2024.173520

[36] Ohba, Y., Shimozaki, T., & Era, H. (2008). Thermoelectric properties of silicon carbide sintered with addition of boron carbide, carbon, and alumina. *Materials Transactions, 49*(6), 1235-1241. https://doi.org/10.2320/matertrans.MRA2007232

[37] Feng, B., Martin, H. P., Hempel-Weber, R., & Michaelis,

A. (2012). Preparation and thermoelectric properties of B4C-Si-B composites. *AIP Conference Proceedings, 1449*, 315. https://doi.org/10.1063/1.4731560

[38] Schierning, G., Chavez, R., Schmechel, R., Balke, B., Rogl, G., & Rogl, P. (2015). Concepts for medium-high to high temperature thermoelectric heat-to-electricity conversion: A review of selected materials and basic considerations of module design. *Translational Materials Research, 2*(2), 025001. https://doi.org/10.1088/2053-1613/2/2/025001